Title
Correcting MIS5e and 5a sea-level estimates for tectonic uplift, an example from southern California

Authors
Simms, Alexander R
Rood, Dylan H
Rockwell, Thomas K

Publication Date
2020-11-01

DOI
10.1016/j.quascirev.2020.106571

Peer reviewed

Correcting MIS5e sea-level estimates for tectonic uplift, an example from southern California

Alexander R. Simms, Dylan H. Rood, and Thomas K. Rockwell

Abstract

Along tectonically active margins, the difference in elevations between global sea levels during highstands and uplifted marine terraces is a function of both tectonics and glacial-isostatic adjustment (GIA). However, disentangling the relative influence of these two processes remains a challenge for those trying to gain insights into either process. In this study, we outline a strategy for isolating the tectonic contribution to marine isotope stage (MIS) 5e and 5a marine terrace elevations for the southern California coast by determining the cosmogenic radionuclide burial age and elevation of the middle Pleistocene (1.48±0.17 Ma) Clairemont Terrace in San Diego. Using this older terrace as a datum for calculating tectonic uplift rate provides a much longer time period to average out uncertainties in past local or relative sea levels (RSL) that arise from ambiguities in GIA parameters and global meltwater volumes. The assumption of constant uplift rates is warranted for this portion of the California coast given its relatively simple tectonic setting on the rift flank of the Salton Trough. From this approach, we determine an average uplift rate of 0.066 ± 0.020 mm/yr or 0.055± 0.013 mm/yr, depending on the RSL model used for the time of the Clairemont Terrace formation, for much of the San Diego coastline. Correcting for this tectonic uplift rate leaves an estimate of 15.1 +2.6/-3.1 m (16.4 +1.9/-2.6 m) and 4.8 ± 1.9 m (5.6 ± 1.5 m) for RSL during MIS5e and MIS5a, respectively. These new estimates of MIS5e and MIS5a sea levels along the southern California coast provide important constraints on GIA parameters and former ocean and ice volumes.

Keywords: Interglacials; Pleistocene; Sea-Level Changes; North America; Coastal Geomorphology; Cosmogenic Isotopes

1. Introduction

Accurate reconstructions of past sea-levels within tectonically active margins are important for understanding rates and driving mechanisms of tectonic processes, constraining the distribution of past ice sheets, reconstructing paleogeography, and assessing future impacts of rising sea level in the modern era. Commonly, estimates of vertical tectonic motion are made by calculating the difference between previous highstand terrace elevations and modern sea levels. However, even during past highstands, such as marine isotope stage 5e (MIS5e), 120,000 years ago, glacial-isostatic adjustment (GIA) can create significant deviations between relative sea level (RSL) experienced at a site and the global average ocean-volume change (Lambeck et al., 2012; Creveling et al., 2015). Thus, in tectonically active areas, two unknowns largely contribute to variability in past highstand elevations: tectonics and GIA. One approach to tackling the two-variable problem is to use numerical predictions of GIA to isolate tectonic motion (Creveling et al., 2015; Simms et al., 2016; Stocchi et al., 2018). However, even the best GIA models require data to help determine which model parameters (e.g. Earth rheology, ice model) are most appropriate for modeling the GIA along a specified section of coast.

For the tectonically active southern California Coast, GIA predictions of MIS5e sea levels range from 10-15 m (Muhs et al., 2012; Creveling et al., 2015; 2017; Simms et al., 2016). Are these models accurate? Ideally, the GIA models would be developed and calibrated using highstand elevations from sites without significant tectonic motion, but no sites free of tectonic motion have been identified for the California Coast. Thus, testing these values has remained elusive. What is needed is an independent estimate of MIS5e sea levels along this tectonically active margin. In this study, we outline an approach to estimate tectonic corrections of MIS5e and younger RSLs by using early Quaternary (e.g. 1-2 Ma) marine terraces as datums for tectonic corrections. We do this by providing the first numerical ages for the Clairemont Terrace near San Diego, California (Kern and Rockwell, 1992; Haaker et al., 2016; Fig. 1) using cosmogenic radionuclide (CRN) isochron burial dating (Balco and Rovey, 2008) on deeply buried quartz-rich clasts and sand. This approach is possible in southern California given the tectonic setting of the site within the rift shoulder of the Gulf of California extension (Mueller et al., 2009), which results in a relatively low and constant rate of tectonic uplift. Using such old marine terraces minimizes the relative importance of ambiguities in RSL that arise from uncertainties associated with past ice volumes, Earth models, and the past distribution of ice sheets because the errors associated with these uncertainties are averaged out over an order of magnitude longer time. Thus their impacts in the total uplift rate errors are generally smaller. Using a longer time frame for the uplift correction does leave the analysis open to more error associated with the assumption of constant uplift rates over a longer period of time. However, for southern California, rift shoulder uplift has been ongoing for the past 5-6 Ma (Mueller et al., 2009), the timeframe for rapid opening of the Gulf of California, and thus the assumption of constant uplift rates appears warranted.

2. Background

Glacial-isostatic adjustment refers to the deformation of the solid Earth, its gravitational field, and the oceans to the growth and decay of the global ice sheets (Lambeck and Chappell, 2001; Whitehouse, 2018). Initially thought to only be important near former ice masses, it is becoming more apparent that its influences can be felt even at large distances from the last great ice sheets (Clark et al., 1978; Lambeck and Chappell, 2001; Whitehouse, 2018). Thus, its influences cannot be ignored and likely impacts many other measures of Earth surface processes that use the elevation of past RSLs as a datum, including rates of tectonic uplift (Lambeck et al., 2012; Creveling et al., 2015; Simms et al., 2016) or subsidence (Simms et al., 2013). For the California coast, the elevation of past RSLs has been an important datum for calculating uplift rates from late Quaternary and Holocene marine terraces (Rockwell et al., 1989; 1992; Muhs et al., 1992; 1994; 2002; 2012; 2014; Rockwell et al., 2016). Of these, the most widespread marine terraces used in the calculation of uplift rates have been those correlated to global highstands during MIS5a and MIS5e (Muhs et al., 1992), as these are commonly well-preserved along coasts worldwide. GIA model predictions for the southern California coast suggest that MIS5e RSLs reached between 10-15 m above modern sea level (Muhs et al., 2012; Creveling et al., 2015; Simms et al., 2016), about 1-9 m above the average global ocean volume change of 6-9 m during MIS5e (Kopp et al., 2013). For MIS5a, these predictions vary more widely from -8 to +1 m (Simms et al., 2016; Creveling et al., 2017), which is up to 25-30 m higher than some estimates of average global ocean volume change at that time (Lambeck and Chappell, 2001; Creveling et al., 2017). However, a location free of tectonic motion along the Pacific Coast of North America to test this deviation from global average ocean-volume changes has not been identified.

The California coast is host to all three broad types of plate boundaries: convergent, divergent, and transform. The southern-most ~100 km of the California Coast, including our study area, lies immediately seaward of a zone of extension within the Salton Trough (Elders et al., 1972; Mueller et al., 2009; Fig. 1). As such, it has experienced a remarkably constant rate of slow uplift related to large-scale flexure of the lithosphere since post-Pliocene times (Mueller et al., 2009). This uplift is thought to be driven by broad mantle upwelling associated with rifting beneath the Salton Trough and extending to the south into the Gulf of California (Mueller et al., 2009). Additionally, the entire coastline between La Jolla and Newport Bay is located within an individual crustal block bounded to the north and south by faults (Axen, 1995; Haaker et al., 2017; Fig. 1). This coherent block motion allows for a relatively straight forward approach to tectonic corrections as it appears that no active faults cut the region along the coast north of La Jolla until the Newport-Inglewood fault comes ashore near Newport Beach (Haaker et al., 2017).

The San Diego County coast north of La Jolla to Newport Bay (Fig. 1) contains a nearly horizontal continuous flight of up to 16 marine terraces mappable across ~100 km of the coastline. The upper terraces are known locally as the Lindavista terrace sequence (Kern, 1977; McCrory and Lajoie, 1979; Kern and Rockwell, 1992; Haaker et al., 2016). The flight of terraces reach an elevation of up to 155 m (Haaker et al., 2016). Four of the higher terraces are also capped by prominent beach ridges traceable across most of their extent (Kern and Rockwell, 1992). These beach ridges attain elevations up to 26 m above the terrace platform (Haaker et al., 2016). The Clairemont Terrace is one of these beach-ridge bearing marine terraces and its broad surface is what much of the city of San Diego is built upon. Below the Lindavista terrace sequence are also up to seven lower terraces, the lowest two of which, with shoreline angle elevations around 22-23 m and 9-11 m, are known as the Nestor and Bird Rock terraces, respectively (Kern and Rockwell, 1992; Haaker et al., 2016). These two lowest terraces have been dated using U-series (Muhs et al., 2002) and amino acid racemization (Kern and Rockwell, 1992) techniques to MIS5e and MIS5a, respectively.

Haaker et al. (2016) used differential GPS technology (dGPS) to survey the upper Lindavista terrace platform and shoreline elevations from the San Diego River northwest to Newport Bay (Fig. 1). Northwest from Oceanside, the broad Lindavista terrace sequence, which is cut across weakly consolidated Eocene conglomerate and shale in most of San Diego County, transitions to narrow terraces with distinct risers separating individual platforms where the underlying rock is the resistant San Onofre Breccia. Despite the transition in erosional resistance, terrace width, and terrace gradient (Haaker et al., 2016), the shorelines maintain a nearly horizontal elevation for at least 65 km of the coast (Fig. 1). Across this portion of the coast, the shoreline angle of the Clairement terrace maintains an elevation of 96 to 97 m from the San Diego River to at least as far north as San Onofre, north of which the higher terraces are obscured by development (Haaker et al., 2016). We focused our new dating efforts on this well-developed marine terrace and shoreline.

3. Methods

3.1 Cosmogenic radionuclide burial age dating

Cosmogenic radionuclide (CRN) burial dating techniques utilize *in situ* produced cosmogenic isotopes with different half-lives (e.g., ^{26}Al, $t_{½}$ = 0.7 Ma and ^{10}Be, $t_{½}$ = 1.36 Ma). The simplest case of burial dating assumes that minerals are first exposed to cosmic rays at or near the Earth's surface and then buried to a depth that shields the minerals from significant cosmic ray bombardment (Granger and

Muzikar, 2001). The production rates of different cosmogenic isotopes in exposed surface material has a constant ratio ($^{26}Al/^{10}Be$ = 6.75, hereafter called production ratio), and if this material is then buried deeply and rapidly so that production ceases, the $^{26}Al/^{10}Be$ ratio decreases in a predictable way over time as the two isotopes radioactively decay at different rates. Thus, the ratio of the two isotopes provides a method of determining how long the sediments have been buried.

However, burial dating of sediment using cosmogenic isotopes is often complicated or rendered impossible by geologic uncertainties including unknown post-burial isotope production and an inherited inventory (Granger and Muzikar, 2001; Granger, 2006). Recently, isochron methods have made some of these geologic uncertainty issues easier to deal with (Balco and Rovey, 2008; Balco et al., 2009). A variation of the isochron dating approach described by Balco and Rovey (2008) makes use of the common post-burial history of a series of samples collected from the same depth horizon, such as in a fluvial or marine terrace, that experienced different amounts of exposure at the landscape surface immediately prior to burial (i.e., individual clasts or multiple grain sizes with different amounts of pre-depositional exposure, hereafter called variable inheritance). Subsequent to burial, each sample experiences some additional nuclide production as secondary cosmic-ray particle energy, neutrons and muons depending on amount of burial, gradually attenuate with depth. However, the relative change in isotope inventories among the different samples is the same for every sample at the same depth interval. For example, the ^{10}Be and ^{26}Al concentrations from samples collected at the same depth, but with variable inheritance, in a sedimentary deposit are linearly related. The slope of a line fit through such samples, plotted in ^{10}Be-^{26}Al space, is a function of the unique production rates and decay constants of ^{10}Be and ^{26}Al, any post-depositional isotope production, and the variable inheritance for each sample. The slope of the line is used as an isochron-dating algorithm (Balco and Rovey, 2008) to calculate the time of burial.

For this study, we sampled two marine terrace sites close to the relic beach shorelines in road cuts with about 10 m of littoral sand and gravel overlying the abrasion platform (Fig. 2). Evidence for the littoral nature of the sands and gravels included the presence of pholad borings in the cobbles, the well-rounded nature of the oblate, spheroid cobbles, the generally well sorted nature of the sands, and the well-developed stratification of the sands and cobbles. We collected samples from deeply-buried sedimentary deposits that contained material appropriate for cosmogenic isochron burial dating, i.e., a bed that contained sediment with a grain size range from sand to cobbles (Fig. 2). This strategy maximized the likelihood that we would sample materials with variable inheritance, but the same post-depositional exposure history. All samples were collected from sediments sourced from quartz-bearing (e.g. granitic) rock types, including sand, small gravel, and up to seven individual, large quartz-bearing clasts (beach cobbles) for analysis.

Sample preparation chemistry was completed in laboratories at the Scottish Universities Environmental Research Centre (SUERC). We isolated and purified quartz, and extracted the Be and Al for cosmogenic isotope analysis from each sample using established isotope dilution chemistry methods (Corbett et al., 2016). Each batch of quartz samples was extracted together with a blank (i.e. carrier only) sample to monitor and correct for laboratory backgrounds. We completed ^{10}Be and ^{26}Al isotopic ratio analyses at the accelerator mass spectrometry (AMS) laboratory at SUERC (Xu et al., 2015). AMS data were used to calculate isotope concentrations (Table S1), which were then used to model isochron burial ages (Fig. 3). Cosmogenic isochron burial ages were calculated using methods described in Bender et al. (2016).

3.2 Uplift rate calculations

We estimated uplift rates (R_U) based on the elevations of the shorelines within the Clairemont Terraces using the following equation:

$$R_U = (E_{cl} – SL)/t \quad (1)$$

where E_{cl} is the elevation in meters of the Clairemont Terrace shoreline and SL is the elevation in meters of sea level at the time (t) of terrace formation. As very few estimates for sea levels exist for 1.5 Ma (e.g. Pedoja et al., 2014), we estimated the elevation of SL at the time of terrace formation by appealing to the oxygen isotope stack of Lisiecki and Raymo (2005) in two ways. First, the $\delta^{18}O$ values of all the highstands within the interval encompassed by the age error range were averaged with 2 standard deviations used as a parameter in the error estimate (ε_{HSL})(Table 1). We also considered a second SL model in which we assumed SL was the highest of the SL highstands during the time period of the terrace formation (14.5 m, Table 1). The ε_{HSL} of the second model was assumed to be the $\delta^{18}O$ error of the Lisiecki and Raymo (2005) stack. The $\delta^{18}O$ value was converted to SL based on the equation:

$$SL = -73*(\delta^{18}O) + 251 \quad (2)$$

from Spratt and Lisiecki (2016). The error for the SL elevation estimate at the time of terrace formation was determined by combining the highstand SL uncertainty (ε_{HSL}) with an unknown contribution from GIA (ε_{GIA}). As determining a GIA estimate for the early Quaternary relies on many unknowns (e.g. ice sheet distribution, size, timing and style of growth and decay, sediment loading, etc.), we start with the assumption that the variability in GIA contributions would be similar to the most recent highstand (MIS5e) of 2-4 m according to the calculations of Creveling et al. (2015) and 4.3-6.4 m according to the calculations of Simms et al. (2016) for Point Loma (San Diego), California depending on the Earth and ice model used. In order to account for any large differences that may have existed between the most recent two glacial ice advances and those during the early Quaternary, we doubled the highest of these values to 12.8 m. However, it should be noted that during a time period with less ice as suggested by the higher $\delta^{18}O$ (Fig. 4; although past temperatures also play an important role), the GIA contribution would be expected to be smaller. The total error for SL estimated at the time of terrace formation (ε_{SL}) is obtained by taking the square root of the squares of those two error estimates:

$$\varepsilon_{SL} = (\varepsilon_{HSL}^2 + \varepsilon_{GIA}^2)^{0.5} \quad (3)$$

The error for the uplift rate then becomes:

$$\varepsilon_{RU} = R_u*([(\varepsilon_{el}^2+ \varepsilon_{SL}^2)^{0.5}/(E_{cl}-SL)]^2+[\varepsilon_t/t]^2)^{0.5} \quad (4)$$

where $\varepsilon_{el \text{ and }} \varepsilon_t$ are the uncertainties in the elevation of the Clairemont Terrace and the errors in the age of the Clairemont Terrace, respectively.

The elevation of relative sea level (RSL) during MIS5e and MIS5a was calculated using the following equation:

$$RSL = E_t – R_u \times t_t \quad (5)$$

Where E_t and t_t are the elevations and ages of the Nestor and Bird Rock terraces, 23 +1/-2 m and 120 ka and 10 ± 1 m and 80 ka, respectively. The error (E_{RSL}) then becomes:

$$E_{RSL} = [(\varepsilon_{ru} \times t_t)^2 + \varepsilon_{et}^2]^{0.5} \quad (6)$$

where ε_{et} is the error in the elevation of the terraces.

3.3 GIA calculations

Our new tectonically corrected MIS5e and MIS5a RSL elevations were compared to the GIA predictions of Simms et al. (2016). Simms et al. (2016) used the CALSEA program of the Australian National University (Nakada and Lambeck et al., 1987; Johnston, 1993; Lambeck et al., 2003; 2012; Lambeck and Purcell, 2005). The ice models used included the Greenland ice model of Fleming and Lambeck (2004), the European ice model of Lambeck et al. (2010), the North American Ice sheets (Laurentide and Cordilleran) of Lambeck et al. (2017), the alpine glaciers as discussed in Lambeck and Purcell (2005), and an Antarctic Ice sheet based on the model discussed in Lambeck et al. (2014). The Earth model parameters considered include upper-mantle viscosities ranging from 1 to 5 x 10^{20} Pa·s, lower mantle viscosities ranging from 7 to 50 x 10^{21} Pa·s, and lithospheric thicknesses ranging from 50 to 100 km (Simms et al., 2016; Fig. 5). Simms et al. (2016) also assumed a global SL volume of +6 m during MIS5e and -15.2 m during MIS5a. We also explored the impacts of increasing and decreasing the amount of ice within the North American Ice sheets by changing the amount of ice at the LGM (for the time period between 45 ka and the start of the deglaciation) and during the stadials MIS5d (~110 ka) and MIS 5b (~94 ka) between MIS5e and MIS5a within our model setup. Any change in global meltwater contributions by changing the amount of ice within the North American ice sheets was compensated by changes in the volume of ice within the far-field ice sheets (e.g. Antarctica) such that the total volume of water in the oceans was the same for each model run.

4. Results

4.1 New marine terrace ages

We obtained two ages of the Clairemont Terrace shoreline deposits. The age from our first site, Torrey Pines (TP), was 1.53±0.11 Ma (2σ)(Fig. 3 and S1). The age at the second site, Ardath Road (AR), was 1.43±0.13 Ma (2σ)(Fig. 3 and S2). The two are within error. For our uplift calculations we used their average age (1.48±0.17 Ma).

4.2 SL estimate for the time of terrace formation.

A RSL estimate for the California coast at the time of the formation of the Clairemont Terrace is still needed to determine uplift rates independent of MIS5a and MIS5e RSLs. According to the $\delta^{18}O$ stack of Lisiecki and Raymo (2004), the time period encompassed by the age and age error of the Clairemont Terrace includes 9 different sea-level highstands ranging in elevations from -14.7 to 14.5 m (Fig..4) when converted to sea level using the equation of Spratt and Lisiecki (2016; Table 1). We therefore consider two RSL models for calculating uplift rates based on the elevation of the Clairemont Terrace: the average highstand model and the maximum highstand model. The average highstand model uses the average elevation of these highstands, which is -0.6 m with a 2σ error of 20.0 m, a value that encompasses the square root of the sum of the squares of the $\delta^{18}O$ composite errors (Table 2). We use the larger of these two values as our ε_{HSL} error (20.0 m). Adding the uncertainty for GIA estimates (12.8 m) yields a total error (ε_{SL}) of 23.7 m. RSL for the average highstand model with errors thus becomes -0.6 ± 23.7 m. For the maximum highstand model we assume that the highstand represents the highest sea level reached during the time encompassed by the ages, 14.5 ± 13.8 m (Table 1).

Although very few geologic estimates for any dated 1.5 Ma shoreline elevation exist, the estimates based on the $\delta^{18}O$ stack of Lisiecki and Raymo (2004) appear to fall within those few existing records. For example, Cronin (1980) estimates values of 13 ± 9 m, 24 ± 11 m, and 16.5 ± 10.5 m for early Pleistocene (~1.0 to 1.8 Ma based on biostratigraphy) sea levels based on shorelines across three portions of the southeastern USA states of North and South Carolina – regions which fit within a similar GIA field as the Pacific Coast of the United States (Creveling et al., 2017).

4.3 Uplift rates and relative sea levels

Based on the new ages of the Clairemont Terrace, the uplift rate along the San Diego Coast is 0.066 ± 0.020 mm/yr using the average highstand model and 0.055 ± 0.013 mm/yr using the ,maximum highstand model (Table 2). Correcting the elevation of the Nestor Terrace for this uplift and using the average highstand model suggests MIS5e RSLs along the San Diego Coastline were 15.1 +2.6/-3.1 m using an age of 120 ka and an elevation of 23+1/-2 m for the terrace (Kern and Rockwell, 1992; Muhs et al., 2002; Table 2). Using the maximum highstand model yields a result of 16.4+1.9/-2.6 m for MIS5e sea levels. This elevation is considerably higher than the global average of 6-9 m during MIS5e (Kopp et al., 2013) but within the range of elevations predicted by GIA models (Fig. 5). Similarly, the same exercise for the MIS5a shoreline results in a local RSL of 4.8 ± 1.9 m, using an elevation and age of 10 ± 1 m and 80 ka, respectively, for the MIS5a-aged Bird Rock terrace (Ku and Kern, 1974; Kern and Rockwell, 1992; Muhs et al., 2002). The maximum highstand model is 0.8 m higher at 5.6 ± 1.5 m (Table 2). This elevation is considerably higher than global sea levels at this time but only 1.6-2.8 m higher than the range of GIA predictions (-1.9 ± 3.2 m)(Simms et al., 2016).

5. Discussion

5.1 Impact of using a middle Pleistocene marine terrace

Using an older marine terrace in the calculation of uplift rates results in the importance of uncertainties related to previous sea levels (e.g. GIA model uncertainties, ocean volume uncertainties, etc.) to diminish. For every 10 m of RSL difference at 1.5 Ma, the tectonically corrected RSL change is only 0.8 m for MIS5e and 0.6 m for MIS5a. For example, the difference in SL estimates for our two different models is 15.6 m (Table 2). Despite such a large difference, it results in an uplift rate estimate difference of only 0.011 mm/yr and a MIS5e RSL estimate difference of only 1.2 m. Such error bars are within the usual limits of the field observations (e.g. the error on the elevation of the MIS5e terrace is +1/-2 m).

One process that does result in larger uncertainties with greater amounts of time is dynamic topography (Moucha et al., 2008; Mitrovica et al., 2020). Published estimates of dynamic topography at Pleistocene timescales for the Pacific Coast of the USA are limited. One global model of dynamic topography by Austermann et al. (2017) suggests rates of vertical motion due to dynamic topography along the Pacific Coast of North America are generally on the order of less than 10 m/Ma (Austermann et al., 2017). Until better models of dynamic topography are formulated we are not able to determine what portion of the 0.066 ± 0.020 mm/yr (0.055 ± 0.013 mm/yr for the maximum uplift model) of uplift experienced along the San Diego coastline is dynamic topography versus rift-shoulder uplift. Distinguishing between dynamic topography and active tectonics is not important for the sea-level reconstruction, but is important for understanding the nature and rates of active tectonic processes.

5.2 Implications for GIA models

Our new uplift rates of 0.066 ± 0.020 mm/yr for the average highstand model and 0.055 ± 0.013 mm/yr for the maximum highstand model are both half of the originally reported rate of 0.13 to 0.14 mm/yr for the MIS5e terrace by Kern and Rockwell (1992) and an even smaller fraction (1/8) if using only the MIS5a terrace. However, this previous study, based on the elevation and age of a dated MIS5e shoreline, did not account for GIA. When correcting for GIA, the rate of uplift based on the same dated MIS5e shoreline is 0.09 ± 0.03 mm/yr and 0.12 ± 0.06 mm/yr for the MIS5a shoreline (Simms et al., 2016), which is within error, although on the higher end, of our new results. Thus, our new estimate for the elevation of the MIS5e shoreline of 15.1 +2.6/-3.1 m for the average highstand model or 16.4 +1.9/-2.6 m for the maximum highstand model and the MIS5a shoreline of 4.8 ± 1.9 m for the average highstand model or 5.6 ± 1.5 m for the maximum highstand model provide important benchmarks for GIA model predictions for the West Coast of North America.

One challenge for predicting RSL from GIA models is the tradeoff between Earth and ice models. In many cases, both parameters are unknowns in the sea-level equation (Lambeck and Chappell, 2001). The new uplift rates produce elevations for the MIS5e and MIS5a marine terraces that are within error of recent GIA predictions for MIS5e, although within the upper range of the error estimates, and only slightly higher than GIA predictions for MIS5a (Fig. 5). One way to improve the fit between observations and GIA predictions is refining the Earth or ice models such that predictions of RSL during MIS5e and MIS5a are higher. Of the Earth model parameters explored by Simms et al. (2016), those Earth models with upper mantle viscosities of 2×10^{20} Pa·s (Fig. 5A) and 4×10^{20} Pa·s result in higher predictions of relative sea levels for MIS5e and MIS5a, respectively. Those Earth models with a thicker lithosphere or higher lower mantle viscosities also lead to higher predictions of RSL during MIS5e and MIS5a (Fig. 5). A thicker lithosphere and a higher lower mantle viscosity result in higher sea levels across southern California as they shift the forebulge associated with the North American ice sheets to the south (Creveling et al., 2017) to beneath our study area. A similar effect on MIS5e and MIS5a sea levels across southern California is induced by changing the size of the North American Ice Sheet. Decreasing the ice during the stadials between MIS5a and MIS5e results in higher MIS5a sea levels and only minor decreases in MIS5e sea levels (Fig. 5). Higher sea levels during both MIS5e and MIS5a are produced with more ice within the North American Ice Sheets during the LGM (Fig. 5).

Alternatively, increasing the global meltwater volumes in the oceans during MIS5e and MIS5a could also bring more agreement between observations and predictions. For our model predictions, we assumed a MIS5e global meltwater volume of +6 m during MIS5e and -15.2 m during MIS5a. Other studies have favored higher sea levels during these times. O'Leary et al. (2012) favor a global meltwater value of 9 m for MIS5e rather than the +6 m used by Simms et al. (2016). Similarly, another recent GIA study by Creveling et al. (2017) suggest that global meltwaters during MIS5a were as high as -8.5±4.6 m. A fourth possible mechanism for increasing MIS5e and MIS5a sea levels could be sediment loading (Simms et al., 2013; Pico, 2019). However, according to one modelling study, rapid sediment loading and erosion along the California margin would provide the opposite affect and lower RSLs (Pico, 2019). Thus, sediment loading and erosion is either expressed differently than modeled by Pico (2019) or requires a larger change in the other potential factors to compensate for those impacts. Given the uncertainties associated with our fundamental assumption of constant uplift rate over the last 1.5 Ma, we feel the small difference between the GIA predicted and uplift-corrected MIS5e and MI5a elevations are not meaningful enough on their own to warrant further speculation as to improvements on Earth models, ice models, or global meltwater volumes. However, if similar observations are made throughout the region or world, these trends may provide insights into improving these parameters.

5.2 Implications for local tectonics

The low rate of uplift of the coastline for this region further supports earlier notions of a relatively simple tectonic overprint for this portion of the coast (Haaker et al., 2016). The uplift of the MIS5 terraces documented by Haaker et al. (2016) decrease in elevation into the Los Angeles basin, reaching their lowest elevation at Newport Bay. This is coincident with the northern end of the Salton Trough, northwest of which the San Andreas Fault is transpressive. Hence, there appears to be a direct correlation between uplift rate and oblique rifting of the Gulf. Thus, the uplift is attributed to, and the rate is consistent with, rift shoulder uplift due to spreading in the Gulf of California and the Salton Trough (Mueller et al., 2009).

A blind thrust fault, the Oceanside Blind Thrust (OBT), has been inferred to exist offshore and project beneath the San Diego County coastline based on vintage offshore seismic lines (Rivera et al., 2000)(Fig. 1). Rivera et al. (2000) attribute the San Joaquin Hills in Orange County to be the result of this blind thrust system. In their model, they segment the OBT, which requires some differential uplift and folding of the coast. However, the observed low rate of uplift does not support the OBT model projecting beneath the coastline (Rivera et al., 2000). Not only is the uplift rate low, but Haaker et al. (2016) demonstrated that there is virtually no folding or differential uplift of the coastal terraces. We dated the Claremont terrace near its paleo-shoreline, and from at least the San Diego River northwest to San Onofre, the terrace shoreline maintains an elevation of 96-97 m, which is essentially flat (Fig. 1). Considering its age of ~1.5Ma, this is evidence for a remarkably stable, regional coastal uplift signal. The only place where this rate is elevated is where the coast is crossed by the Rose Canyon fault in La Jolla (Fig. 1). Here, the MIS5 terraces are elevated by only a few meters (Kern and Rockwell, 1992). These observations imply that the primary seismic hazard for the San Diego region is from the strike-slip faults along the coast and offshore. Furthermore, no evidence can be found for uplift related to shortening and blind thrusting, which should not only produce a distinct uplift signal, but based on the inferred segmentation of the Oceanside Blind Thrust, should produce differential uplift and folding of the coastal terraces. Such uplift and folding of coastal terraces is not observed (Haaker et al., 2016).

Finally, our estimates of MIS5 RSL will invariably decrease all published uplift rates derived from coastal terrace data in southern California and adjacent northern Baja California. The relative importance of these corrections to the tectonic uplift rate are somewhat dependent on the amount of uplift. Coasts that are rising slowly are more sensitive to our refinement of MIS5e and MIS5a RSLs, while those that are uplifting more rapidly are less sensitive to the adjustment to MIS5e and MIS5a RSLs. For instance, Rockwell et al. (1989) mapped and dated marine terraces from Punta Banda in northern Baja California and inferred an uplift rate as high as 0.31 mm/yr but assumed a RSL of +6m during MIS5e. Using our RSL for MIS5e of 15 m lowers the uplift rate to 0.23 mm/yr. For regions such as the axis of the Ventura Avenue Anticline near Ventura, California where the MIS5a marine terrace projects to an elevation of more than ~625 m (Rockwell et al., 1988; 2016), our refinement of ~20 m only reduces the uplift rate from 8.0 mm/yr to 7.7 mm/yr. However, the inferred average rate of uplift for most of the southern California coast is relatively low, with published rates typically in the 0.13 to 0.2 mm/yr range (although higher in some areas of the Transverse Ranges; Rockwell et al., 2016). At these low rates, our new estimates of RSL will have the effect of dropping the inferred uplift rates by as much as a half, which for some tectonic models, will be significant.

6. Conclusions

Using the age of the Clairemont Terrace, 1.48+0.17 Ma, we find that the Lindavista Terraces of southern California are uplifting at a rate of 0.066 ± 0.020 mm/yr for the average highstand model or 0.055 ± 0.013 mm/yr for the maximum highstand model. This uplift rate places the elevations of RSL for the MIS5e and MIS5a marine terraces at 15.1 +2.6/-3.1 m or 16.4 +1.9/-2.6 m (depending on highstand models) and 4.8 ± 1.9 m or 5.6 ± 1.5 m (depending on highstand models), respectively. These estimates of relative sea level are within error of recent models of GIA for this portion of the California coast and provide important benchmarks for future GIA model predictions along this tectonically active margin. In general, these new estimates of RSL support GIA modeling studies suggesting that tectonic uplift rates along many portions of the US West Coast are lower than originally reported.

Acknowledgements

The authors would like to thank Kurt Lambeck and Helene Rouby for use of and help with GIA code, and Victoria Forbes and the staff of the Scottish Universities Environmental Research Centre (SUERC) for support during cosmogenic isotope analyses. This manuscript was improved by helpful comments from one anonymous reviewer and Harvey Kelsey. We also thank Jacky Austermann for discussion related to dynamic topography along the Pacific coast but acknowledge that any mistakes are those of the authors and not the reviewers.

Figure Captions

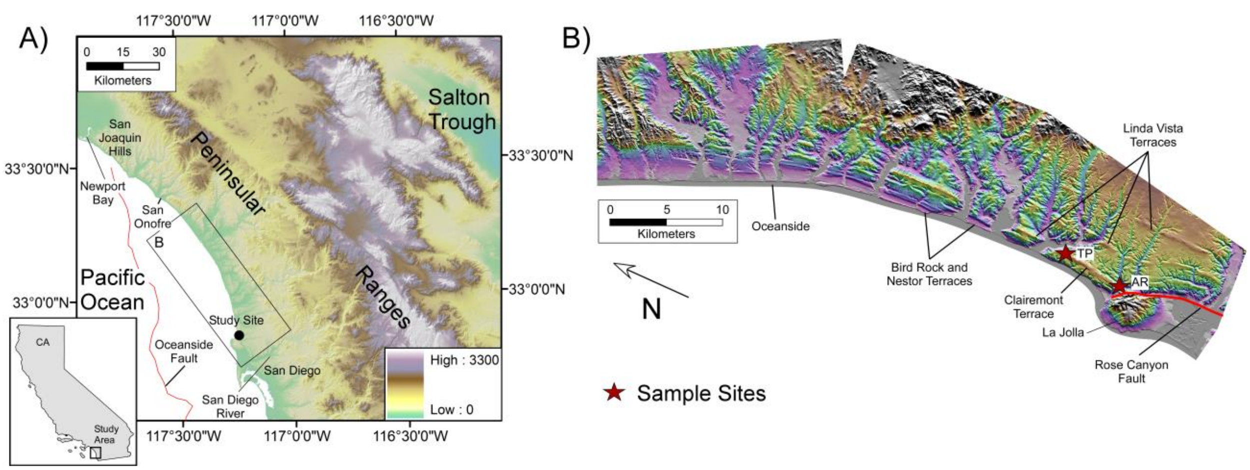

Figure 1. A) Map of the study area with an inset showing the general location within the state of California. B) Digital elevation model of the Lindavista Terraces (from Haaker et al., 2016) including the location of sample sites Torrey Pine (TP) and Ardath Road (AR) as well as other features mentioned in the text.


A.
B.

Figure 2. Photograph of the shoreline deposits overlying the Clairemont Terrace dated as part of this study at the Torrey Pine (TP) site (A.) and the Ardath Road (AR) site (B.). 2 m survey rod for scale.

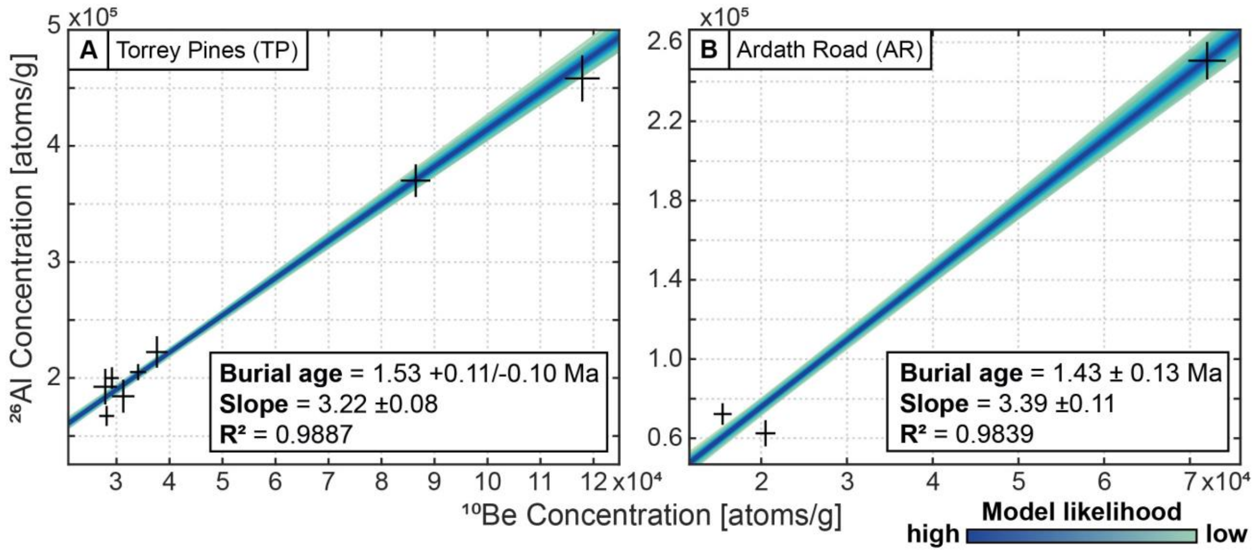

Figure 3. ^{26}Al-^{10}Be isochron burial dating results for TP (left) and AR (right) sites showing individual samples with 1σ error crosses and Bayesian linear regression fits color-coded by likelihood. Summary text gives modal (most likely) estimate and 1σ errors for slope and y-intercept. Slope regression and error analysis give a burial age of 1.53 +0.11/-0.10 Ma (95% CI; N=8, excluding no outliers) for the TP site, and 1.43 +/- 0.13 Ma (95% CI; N=3, excluding 1 outlier AR-A) for the AR site.

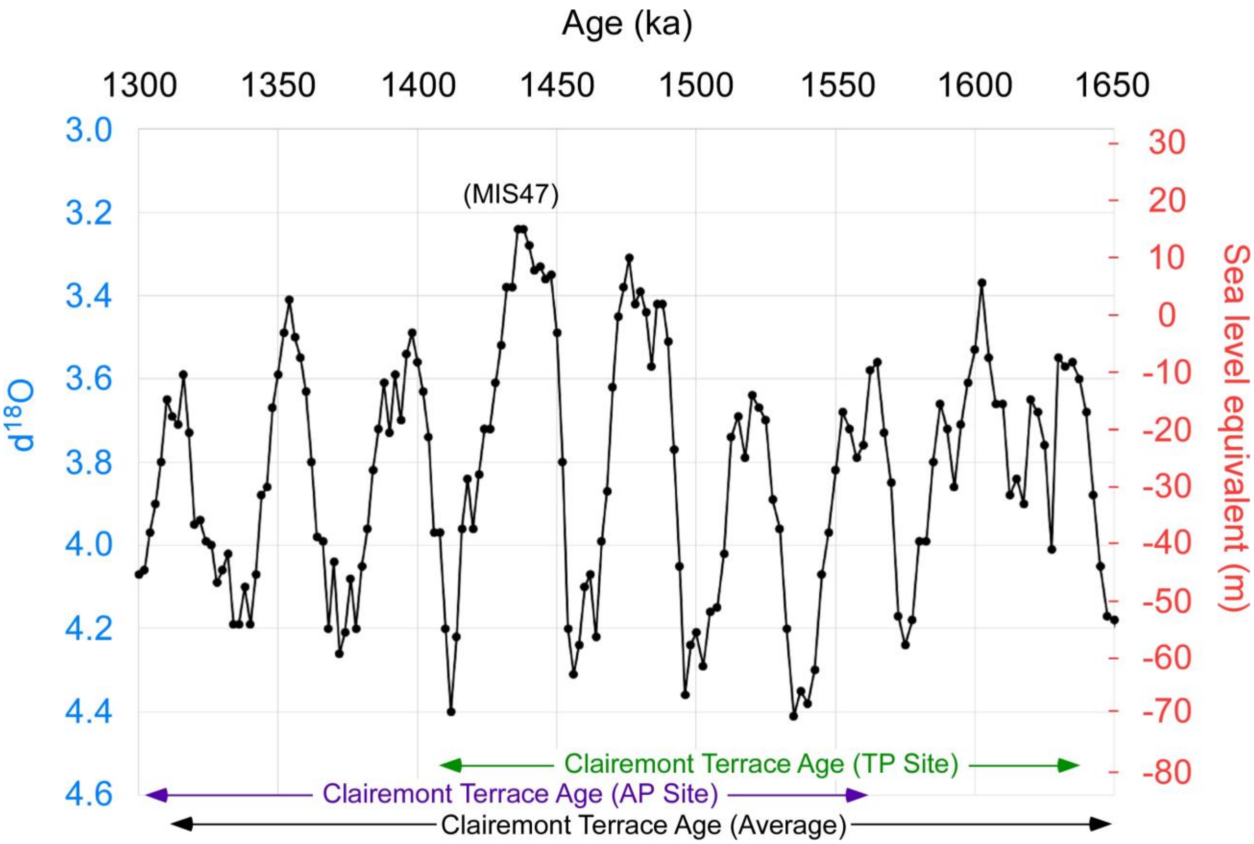

Figure 4. The $\delta^{18}O$ stack of Lisiecki and Raymo (2005) over the time period encompassed by the error range of the cosmogenic burial ages obtained from the Clairemont Terrace. Also shown is the sea-level equivalent using the conversion from $\delta^{18}O$ to sea level from Spratt and Lisiecki (2016) as well as the cosmogenic radionuclide burial ages obtained from the Clairemont Terrace.

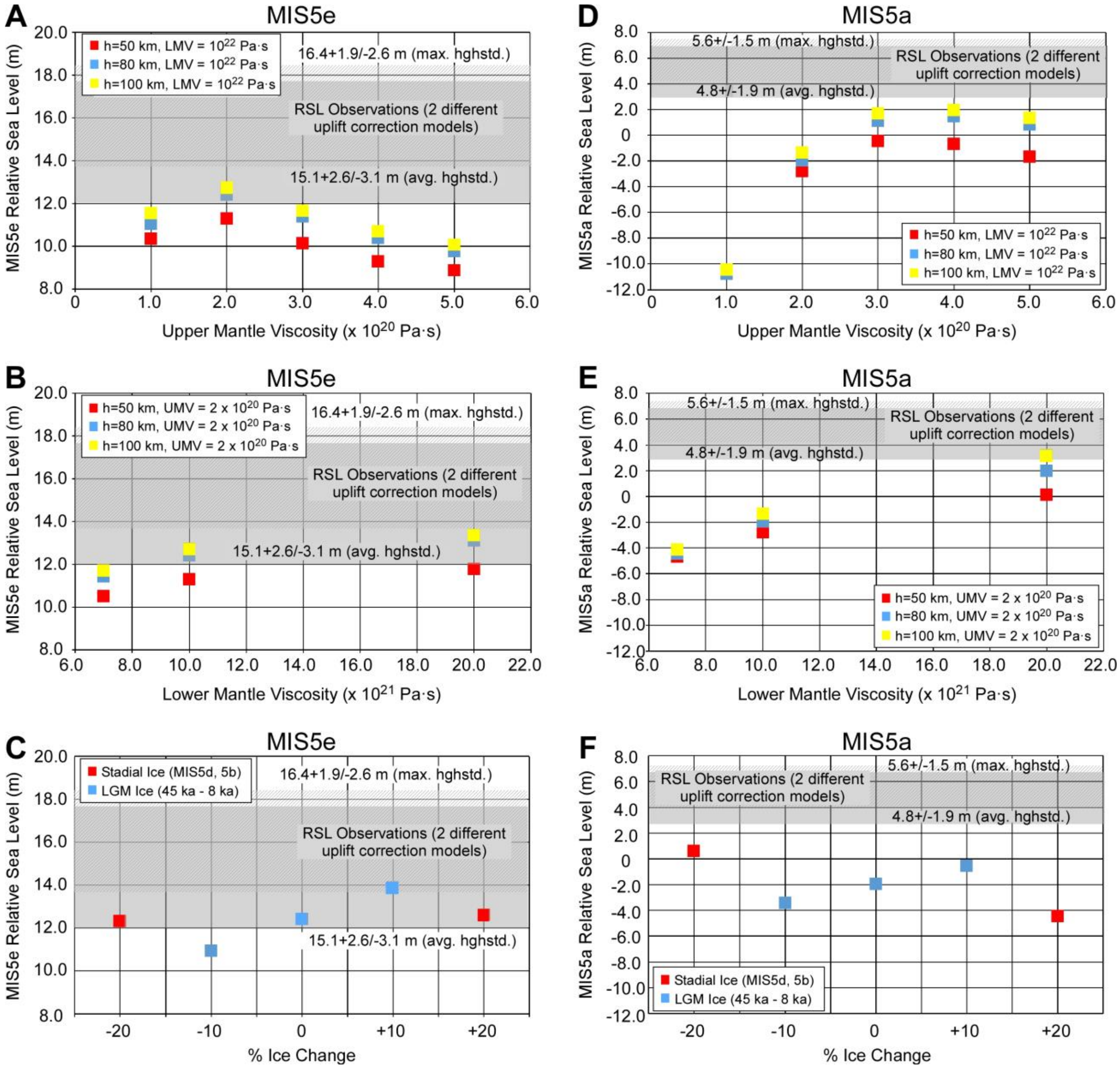

Figure 5. GIA predictions of MIS5e (A-B) and MIS 5a (D-E) relative sea levels at Point Loma (San Diego), California as a function of (A, D) upper mantle viscosity (UMV) and (B, E) lower mantle viscosity (LMV) for 3 different Earth models with lower mantle viscosities (LMV) of 10^{22} Pa·s (A, D), upper mantle viscosities of 2 x 10^{20} Pa·s (B, E), and lithospheric thicknesses (h) of 50 (red squares), 80 (blue squares), and 100 km (yellow squares) compared to MIS5e (A-B) and MIS5a (D-E) observations corrected for tectonics. Gray and hashed rectangles indicate the area within the error bars of the MIS5e (A-C) and MIS5a (D-F) RSL observations using the average highstand model- (avg. hghstd.) and maximum highstand model- (max. hghstd.) derived tectonic corrections, respectively. See text for a description of the two models. C.) and F.) Same as A.) and D.) but as a function of changes in the size of the North American Ice Sheets during the Last Glacial Maximum (LGM) and during MIS5d (~110 ka) and MIS5b (~94 ka) using an Earth model with a lithospheric thickness of 80 km, upper mantle viscosity of 2 x 10^{20} Pa·s, and a lower mantle viscosity of 10^{22} Pa·s. The total global sea-level function is conserved for these scenarios such that any changes in global sea-level volumes induced by changing the size of the North

American Ice Sheet is compensated by far-field (e.g. Antarctica) ice-sheet contributions. GIA model predictions from Simms et al. (2016).

Table 1. Sea-level estimates for the time period encompassed by the Clairemont Terrace Ages.

Age* (ka)	$\delta^{18}O^{\wedge}$ (‰)	Error (‰)	$SL^{\&!}$ (m)	$Error^{\#}$ (m)
1316	3.59	0.05	-11.1	3.6
1354	3.41	0.06	2.1	4.4
1398	3.49	0.05	-3.8	3.6
1438	3.24	0.07	14.5	5.1
1476	3.31	0.08	9.4	5.8
1520	3.64	0.07	-14.7	5.1
1565	3.56	0.05	-8.9	3.6
1602.5	3.37	0.04	5.0	2.9
1630	3.55	0.06	-8.1	4.4

*Ages of the highstands encompassed by the cosmogenic burial ages of the Clairemont Terrace

$^{\wedge}$Lisiecki and Raymo (2005)

$^{\&}$Using the sea-level equation of Spratt and Lisieki (2016)

$^{!}$Average = -0.6 m, Median = -0.9 m, 1 σ = 10.0 m, 2 σ (ε_{HSL}) = 20.1 m

$^{\#}$Square root of the sum of the squares = 13.1 m

Table 1. Sea-level estimates for the time period encompassed by the Clairemont Terrace Ages.

Table 2. Uplift rate calculations

Terrace	Age (ka)	Error (ka)	Elevation (m)	Error (m)	SL (m)	ε_{HSL} (m)	ε_{SL}* (m)	Uplift Rate (mm/yr)	Error (mm/yr)	$RSL^{!}$ (m)	Error (m)
Clairemont (TP Site)	1530	110									
Clairemont (AP Site)	1430	130									
Clairemont	$1480^{\wedge}$	170	96.5	0.5	$-0.6^{\&}$	20	23.7	0.066	0.02		
Clairemont	$1480^{\wedge}$	170	96.5	0.5	$14.5^{\#}$	5.1	13.8	0.055	0.013		
Nestor	120	5	23	+1/-2	$-0.6^{\&}$	20	23.7	0.066	0.02	15.1	+2.6/-3.1
Nestor	120	5	23	+1/-2	$14.5^{\#}$	5.1	13.8	0.055	0.013	16.4	+1.9/-2.6
Bird Rock	80	5	10	1	$-0.6^{\&}$	20	23.7	0.066	0.02	4.8	1.9
Bird Rock	80	5	10	1	$14.5^{\#}$	5.1	13.8	0.055	0.013	5.6	1.5

*ε_{GIA} was assumed to be 12.8 m

!RSL at the time of terrace formation adjusted for the background uplift rate

$^{\wedge}$Average of the TP and AP site ages

$^{\&}$The average RSL from all highstands encompassed by the Clairemont cosmogenic burial ages within the $\delta^{18}O$ stack of Lisiecki and Raymo (2016) converted to sea level using the equation of Spratt and Lisiecki (2016) (The "average highstand model" within the text)

$^{\#}$The RSL of the maximum highstand encompassed by the Clairemont cosmogenic burial ages within the $\delta^{18}O$ stack of Lisiecki and Raymo (2016) converted to sea level using the equation of Spratt and Lisiecki (2016) (The "maximum highstand model" within the text)

Table 2. Uplift rate calculations

Supplementary Information

Table S1: Cosmogenic radionuclide (CRN) sample data and calculations of inputs for isochron burial dating.

Figure S1: CRN isochron burial dating results from Torrey Pines (TP).

Figure S2: CRN isochron burial dating results from Ardath Road (AR).

References:

Austermann, J., Mitrovica, J.X., Huybers, P., and Rovere, A., 2017, Detection of a dynamic topography signal in last interglacial sea-level records: Science Advances, v. 3, e1700457.

Axen, G. J., 1995, Extensional segmentation of the Main Gulf Escarpment, Mexico and United States: Geology, v. 23, p. 515-518.

Balco, G., and Rovey, C. W. I., 2008, An isochron method for cosmogenic-nuclide dating of buried soils and sediments: American Journal of Science, v. 308, p. 1083.

Balco, G., and Shuster, D. L., 2009, Al-26 - Be-10 - Ne-21 burial dating: Earth and Planetary Science Letters, v. 286, p. 570-575.

Bender, A. M., Amos, C. B., Bierman, P. R., Rood, D. H., Staisch, L., Kelsey, H. M., and Sherrod, B., 2016, Differential uplift and incision of the Yakima River terraces: Journal of Geophysical Research: Solid Earth, v. 121.

Clark, J. A., Farrell, W. E., and Peltier, W. R., 1978, Global changes in postglacial sea level: a numerical calculation: Quaternary Research, v. 9, p. 265-287.

Corbett, L. B., Bierman, P. R., and Rood, D. H., 2016, An approach for optimizing in situ cosmogenic ^{10}Be sample preparation: Quaternary Geochronology, v. 33, p. 24-34.

Creveling, J. R., Mitrovica, J. X., Clark, P. U., Waelbroeck, C., and Pico, T., 2017, Predicted bounds on peak global mean sea level during marine isotope stages 5a and 5c: Quaternary Science Reviews, v. 163, p. 193-208.

Creveling, J. R., Mitrovica, J. X., Hay, C. C., Austermann, J., and Kopp, R. E., 2015, Revisiting tectonic corrections applied to Pleistocene sea-level highstands: Quaternary Science Reviews, v. 111, p. 72-80.

Cronin, T.M., 1980, Biostratigraphic correlation of Pleistocene marine deposits and sea levels, Atlantic coastal plain of the southeastern United States: Quaternary Research, v. 13, p. 213-229.

Dyke, A.S., and Peltier, W.R., 2000, Forms, response times and variability of relative sea-level curves, glaciated North America: Geomorphology, v. 32, p. 315-333.

Elders, W. A., Rex, R. W., Robinson, P. T., Biehler, S., and Meidav, T., 1972, Crustal spreading in Southern California: Science, v. 178, p. 15-24.

Fleming, K., and Lambeck, K., 2004, Constraints on the Greenland ice sheet since the Last Glacial Maximum from sea-level observations and glacial rebound models: Quaternary Science Reviews, v. 23, p. 1053-1077.

Granger, D., 2006, A review of burial dating methods using Al-26 and Be-10, *in* Siame, L., Bourles, D., and Brown, E., eds., In-Situ-Produced Cosmogenic Nuclides and Quantification of Geological Processes: Boulder, CO, Geological Society of America.

Granger, D., and Muzikar, P., 2001, Dating sediment burial with in situ-produced cosmogenic nuclides: theory, techniques, and limitations: Earth and Planetary Science Letters, v. 188, p. 269-281.

Haaker, E. C., Rockwell, T. K., Kennedy, G. L., Ludwig, L. G., Freeman, S. T., Zumbro, J. A., Mueller, K. J., and Edwards, R. L., 2016, Style and rate of long-term uplift of the Southern California coast between San Diego and Newport Beach with potential implications for assessing blind thrust models, *in* Anderson, R. Y., and Ferriz, H., eds., Applied Geology in California, Volume 26, Association of Environmental and Engineering Geologists (AEG), p. 679-720.

Johnston, P., 1993, The effect of spatially non-uniform water loads on the prediction of sea-level change: Geophysical Journal International, v. 114, p. 615-634.

Kern, J. P., 1977, Origin and history of upper Pleistocene marine terraces, San Diego, California: Geological Society of America Bulletin, v. 88, p. 1553-1566.

Kern, J. P., and Rockwell, T. K., 1992, Chronology and deformation of Quaternary Marine shorelines, San Diego County, California, *in* Fletcher, C. H. I., and Wehmiller, J. F., eds., Quaternary Coasts of the United States: Marine and Lacustrine Systems, Volume 48: Tulsa, Oklahoma, SEPM, p. 377-382.

Kopp, R. E., Simons, F. J., Mitrovica, J. X., Maloof, A. C., and Oppenheimer, M., 2013, A probabilistic assessment of sea level variations within the last interglacial stage: Geophysical Journal International, v. 193, p. 711-716.

Ku, T.L., and Kern, J.P., 1974, Uranium-series age of upper Pleistocene Nestor terrace, San Diego, California: Geological Society of America Bulletin, v. 85, p. 1713-1716.

Lambeck, K., and Chappell, J., 2001, Sea level change through the last glacial cycle: Science, v. 292, p. 679-686.

Lambeck, K., and Purcell, A., 2005, Sea-level change in the Mediterranean Sea since the LGM: Model predictions for tectonically stable areas: Quaternary Science Reviews, v. 24, p. 1969-1988.

Lambeck, K., Purcell, A., and Dutton, A., 2012, The anatomy of interglacial sea levels: The relationship between sea levels and ice volumes during the Last Interglacial: Earth and Planetary Science Letters, v. 315-316, p. 4-11.

Lambeck, K., Purcell, A., Johnson, P., Nakada, M., and Yokoyama, Y., 2003, Water-load definition in the glacio-hydro-isostatic sea-level equation: Quaternary Science Reviews, v. 22, p. 309-318.

Lambeck, K., Rouby, H., Purcell, A., Sun, Y., and Sambridge, M., 2014, Sea level and global ice volumes from the Last Glacial MAximum to the Holocene: Proceedings fo the National Academy of Sciences of the United States of America, v. 111, p. 15,296-15,303.

Lisiecki, L. E., and Raymo, M. E., 2005, A Pliocene-Pliestocene stack of 57 globally distributed benthic d18O records: Paleoceanography, v. 20, p. 1-17.

McCrory, P. F., and Lajoie, K. R., 1979, Marine terrace deformation, San Diego County, California (Abstract): Tectonophysics, p. 407-408.

Moucha, R., Forte, A.M., Mitrovica, J.X., Rowley, D.B., Quéré, S., Simmons, N.A, and Grand, S.P., 2008, Dynamic topography and long-term sea-level variations: There is no such thing as a stable continental platform: Earth and Planetary Science Letters, v. 271, p. 101-108.

Mitrovica, J.X., Austermann, J., Coulson, S., Creveling, J.R., Hoggard, M.J., Jarvis, G.T., and Richards, F.D., 2020, Dyanamic topography and ice age paleoclimate: Annual Review of Earth and Planetary Sciences, v. 48, p. 585-621.

Mueller, K., Kier, G., Rockwell, T., and Jones, C. H., 2009, Quaternary rift flank uplift of the Pneinsular Ranges in Baja and southern California by removal of mantle lithosphere: Tectonics, v. 28, p. TC5003.

Muhs, D. R., Kennedy, G. L., and Rockwell, T. K., 1994, Uranium-series ages of marine terrace corals from the Pacific Coast of North America and implications for last-interglacial sea level history: Quaternary Research, v. 42, p. 72-87.

Muhs, D. R., Rockwell, T. K., and Kennedy, G. L., 1992, Late Quaternary uplift rates of marine terraces on the Pacific coast of North America, southern Oregon to Baja California Sur: Quaternary International, v. 15-16, p. 121-133.

Muhs, D. R., Simmons, K. R., Kennedy, G. L., and Rockwell, T. K., 2002, The last interglacial period on the Pacific Coast of North America: Timing and paleocliamte: Geological Society of America Bulletin, v. 2002, p. 569-592.

Muhs, D. R., Simmons, K. R., Schumann, R. R., Groves, L. T., DeVogel, S. B., Minor, S. A., and Laurel, D., 2014, Caostal tectoncis on the eastern margin of the Pacific Rim: late Quaternary sea-level history and uplift rates, Channel Islands National Park, California, USA: Quaternary Science Reviews, v. 105, p. 209-238.

Muhs, D. R., Simmons, K. R., Schumann, R. R., Groves, L. T., Mitrovica, J. X., and Laurel, D., 2012, Sea-level history during the Last Interglacial complex on San Nicolas Island, California: implications for glacial isostatic adjustment processes, paleozoogeography and tectonics: Quaternary Science Reviews, v. 37, p. 1-25.

Nakada, M., and Lambeck, K., 1987, Glacial rebound and relative sea-level variations: A new appraisal: Geophysical Journal of the Royal Astronomical Society, v. 90, p. 171-224.

O'Leary, M. J., Hearty, P. J., Thompson, W. G., Raymo, M. E., Mitrovica, J. X., and Webster, J. M., 2013, Ice sheet collapse following a prolonged period of stable sea-level during the last interglacial: Nature Geoscience, v. 6, p. 796-800.

Pedoja, K., Husson, L., Johnson, M.E., Melnick, D., Witt, C., Pchat, S., Nexer, M., Delcaillau, B., Pinegina, T., Poprawski, Y., Authemayou, C., Elliot, M., Regard, V., and Garestier, F., 2014, Coastal staircase sequences reflecting sea-level oscillations and tectonic uplift during the Quaternary and Neogene: Earth-Science Reviews, v. 132, p. 13-38.

Perg, L. A., Anderson, R. S., and Finkel, R. C., 2001, Use of a new ^{10}Be and ^{26}Al inventory method to date marine terraces, Santa Cruz, California, USA: Geology, v. 29, p. 879-882.

Pico, T., 2019, Towards assessing the influence of sediment loading on Last Interglacial sea level: Geophysical Journal International, v. 220, p. 384-392.

Rivero, C., Shaw, J. H., and Mueller, K., 2000, Oceanside and Thirtymile Bank blind thursts: Implications for earthquake hazards in coastal southern California: Geology, v. 28, p. 891-894.

Rockwell, T., Muhs, D. R., Kennedy, G. L., Hatch, M. E., Wilson, S. H., and Klinger, R. E., 1989, Uranium-series ages, faunal correlations and tectonic deformation of marine terraces within the Agua Blanca fault zone at Punta Banda, northern Baja California, Mexico, *in* Abbott, P. L., ed., Geologic Studies in Baja California: Socety of Economic Paleontologists and Mineralogists Pacific Section, Volume 63, SEPM, p. 1-16.

Rockwell, T. K., Clark, K., Gamble, L., Oskin, M. E., Haaker, E. C., and Kennedy, G. L., 2016, Large Transverse Range earthquakes cause coastal upheaval near Ventura, Southern California: Bulletin of the Seismological Society of America, v. 106, p. 2706-2720.

Rockwell, T.K., Keller, E.A., and Dembroff, G.R., 1988, Quaternary rate of folding of the Ventura Avenue anticline, western Transverse Ranges, southern California: Geological Society of America Bulletin, v. 100, p. 850-858.

Rockwell, T. K., Nolan, F., Johnson, D. L., and Patterson, R. H., 1992, Ages and deformation of marine terraces between Point Conception and Gaviota, Western Transverse Ranges, California, *in* Fletcher, C. H. I., and Wehmiller, J., eds., Quaternary Coast of the United States: Marine and Lacustrine Systems, Volume 48: Tulsa, OK, SEPM, p. 333-341.

Simms, A. R., Anderson, J. B., DeWitt, R., Lambeck, K., and Purcell, A., 2013, Quantifying rates of coastal subsidence since the last interglacial and the role of sediment loading: Global and Planetary Change, v. 111, p. 296-308.

Simms, A. R., Rouby, H., and Lambeck, K., 2016, Marine terraces and rates of vertical tectonic motion: The importance of glacio-isostatic adjustment along the Pacific coast of central North America: Geological Society of America Bulletin, v. 128, p. 81-93.

Spratt, R. M., and Lisiecki, L. E., 2016, A Late Pleistocene sea level stack: Climate of the Past, v. 12, p. 1079-1092.

Stocchi, P., Vacchi, M., Lorscheid, T., De Boer, B., Simms, A. R., Van de Wal, R. S. W., Vermeerson, B. L. A., Pappalardo, M., and Rovere, A., 2018, MIS5e relative sea-level changes in the Mediterranean Sea: Contribution of isostatic disequilibrium: Quaternary Science Reviews, v. 185, p. 122-134.

Whitehouse, P. L., 2018, Glacial isostatic adjustment modelling: historical perspectives, recent advances, and future directions: Earth Surface Dynamics, v. 6, p. 401-429.

Xu, S., Freeman, S. P. H. T., Rood, D. H., and Shanks, R. M., 2015, Decadal ^{10}Be, ^{26}Al and ^{36}Cl QA measurements on the SUERC accelerator mass spectrometer: Nuclear Instruments and Methods B: Beam Interactions with Materials and Atoms, v. 361, p. 39-42.